Angular dependence of the *pp* elastic-scattering analyzing power between 0.8 and 2.8 GeV. II. Results for higher energies

C. E. Allgower,[1] J. Ball,[2,3] M. E. Beddo,[1,*] J. Bystrický,[3] P.-A. Chamouard,[2] M. Combet,[2,3] Ph. Demierre,[4] J.-M. Fontaine,[2,3] D. P. Grosnick,[1,†] R. Hess,[4,‡] Z. Janout,[5,§] Z. F. Janout,[4,‖] V. A. Kalinnikov,[5] T. E. Kasprzyk,[1] B. A. Khachaturov,[5] R. Kunne,[2,¶] F. Lehar,[3] A. de Lesquen,[3] D. Lopiano,[1] M. de Mali,[3,‡] V. N. Matafonov,[5] I. L. Pisarev,[5] A. A. Popov,[5] A. N. Prokofiev,[6] D. Rapin,[4] J.-L. Sans,[2,**] H. M. Spinka,[1] A. Teglia,[4] Yu. A. Usov,[5] V. V. Vikhrov,[6] B. Vuaridel,[4] and A. A. Zhdanov[6]

[1]*HEP Division, Argonne National Laboratory, 9700 South Cass Avenue, Argonne, Illinois 60439*
[2]*Laboratoire National Saturne, CNRS/IN2P3 and CEA/DSM, CEA/Saclay, F-91191 Gif-sur-Yvette Cedex, France*
[3]*DAPNIA, CEA/Saclay, F-91191 Gif-sur-Yvette Cedex, France*
[4]*DPNC, University of Geneva, 24 quai Ernest-Ansermet, CH-1211 Geneva 4, Switzerland*
[5]*Laboratory of Nuclear Problems, JINR, RU-141980 Dubna, Moscow Region, Russia*
[6]*Petersburg Nuclear Physics Institute, RU-188350 Gatchina, Russia*

(Received 1 June 1999; published 15 October 1999)

Measurements at 18 beam kinetic energies between 1975 and 2795 MeV and at 795 MeV are reported for the *pp* elastic-scattering single spin parameter $A_{ooon}=A_{oono}=A_N=P$. The c.m. angular range is typically 60–100°. These results are compared to previous data from Saturne II and other accelerators. A search for energy-dependent structure at fixed c.m. angles is performed, but no rapid changes are observed. [S0556-2813(99)03710-3]

PACS number(s): 13.75.Cs, 13.88.+e, 25.40.Cm

I. INTRODUCTION

This paper reports results from a major experimental program to measure *pp* elastic-scattering spin observables up to a kinetic energy of 2800 MeV at the Saturne II accelerator in Saclay. It is a continuation of the measurements described in the accompanying paper—Ref. [1]. Analyzing power results are presented at 19 energies and compared to earlier data. These results significantly increase the *pp* elastic-scattering data base, and allow a search for rapid energy dependence in this spin observable.

The experiment was performed with a polarized proton beam incident on a frozen-spin polarized proton target in four run periods spread over a three-year time span. Data from the first two run periods (I, II) are described in Ref. [1], and from the last two (III, IV) are presented here. Each run period was 10–14 days in duration, during which measurements were made at a number of energies. Data were collected simultaneously with an unpolarized CH_2 target, and these A_N data are published in Ref. [2]. Results on the spin observables K_{onno} and D_{onon} from these same run periods are given in Ref. [3], and on $A_{oonn}=C_{NN}$ will be published in the future.

About half the data sets in run periods III and IV repeat energies from Ref. [1] in order to search for systematic errors and to allow a cross normalization, if necessary. Most of the remaining data sets are above 2.3 GeV, at energies where no previous data exist. A measurement at 795 MeV is included in order to check the absolute target polarization. Various tests for efficiency changes were performed for all data sets.

Many details of the experimental apparatus are given in Refs. [4–9]. Some changes were made to the hardware for the different run periods, as described in Sec. II and Ref. [1]. A brief description of the data analysis is made in Sec. III, and the results are presented in Sec. IV.

II. EXPERIMENTAL APPARATUS

A. Polarized beam and beam polarimeters

The polarized beam was produced in an atomic beam-type, polarized ion source and accelerated in both the Mimas booster ring and the Saturne II accelerator. Four different beam polarization states were used at most energies during run periods III and IV, designated 0_+ (state 1), $-$ (state 2), $+$ (state 3), and 0_- (state 4). The polarization of the beam pulses normally alternated in the pattern $0_+,-,+,0_-,-,+,0_+,-,+,0_-,\ldots$. The polarization direction during acceleration was vertical, with relative direction given by the $+$ and $-$ signs in the designation of the four states. Certain beam energy ranges had $+$ corresponding to vertically up, and other ranges to vertically down, due to the flipping of the beam spin at certain depolarizing resonances. As described in Ref. [1], the ratios of polarizations were consistent with being constant with magnitudes:

$$P_{0+}:P_-:P_+:P_{0-}=0.072:1.000:1.000:0.072. \quad (1)$$

*Present address: Data Ventures LLC, Los Alamos, NM 87544.
†Present address: Department of Physics and Astronomy, Valparaiso University, Valparaiso, IN 46383.
‡Deceased.
§Present address: Faculty of Nuclear Sciences and Physical Engineering, Czech Technical University, Břehová 7, 11519 Prague 1, Czech Republic.
‖Present address: Computing Center of the Czech Technical University, Zikova 4, 16635 Prague 6, Czech Republic.
¶Present address: Institut de Physique Nucléaire IN2P3, F-91400 Orsay, France.
**Present address: Centrale Themis, F-66121 Targasonne, France.

 ©1999 The American Physical Society

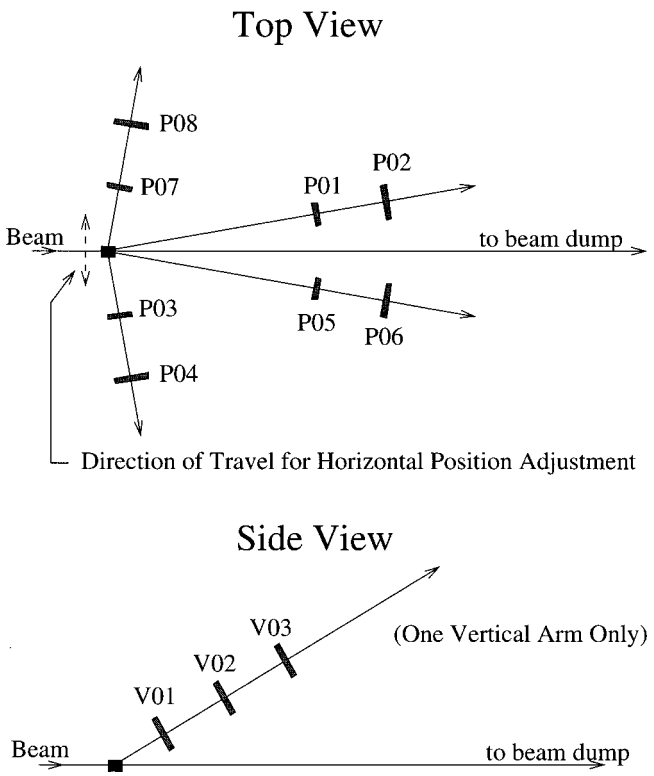

FIG. 1. Top and side view of the downstream polarimeter (not to scale) showing the location of the scintillation counters.

These four magnitudes were then multiplied by a different constant at different times as the ion source polarization varied or the accelerator depolarization changed. These conclusions are partly based on special measurements made subsequent to the experiments described in this paper; see Ref. [10]. The typical size of the beam near the polarized target was measured to be ~ 20 mm in diameter, and the typical magnitude of the beam polarization was 0.6–0.9.

Three relative beam polarimeters were used to monitor the vertical (N-type) and horizontal (S-type) transverse components of the beam polarization. These were the SD3 polarimeter [1,5] located near the Sirène magnet, the target-region or antipolarimeter [1] situated slightly upstream of the polarized target, and the downstream or ''Gatchina'' polarimeter, whose target was 6.54 m downstream of the polarized target. They measured the vertical, horizontal, and vertical components of the beam polarization, respectively.

Another pair of arms was added to the SD3 polarimeter for run periods III and IV, each arm containing two scintillation counters (SP'_3,SP'_4 and SP'_7,SP'_8) in the horizontal plane. These arms were fixed, and allowed the ''on'' and ''off'' kinematics data to be collected simultaneously. The fourfold coincidences $L'_c = SP_1 \cdot SP_2 \cdot SP'_3 \cdot SP'_4$, $R'_c = SP_5 \cdot SP_6 \cdot SP'_7 \cdot SP'_8$, and the corresponding accidentals were generated and scaled in addition to L_c, and R_c; see [1]. In these two run periods, the CH_2 polarimeter target was used for nearly all data collection with the beam incident on the polarized target for the elastic-scattering measurements. The carbon polarimeter target results were taken while the target polarization was being measured and reversed. In this case, the beam stop near the Alizé magnet was closed, so that no beam entered the experimental area, and the beam intensity on the SD3 polarimeter was increased somewhat by opening the adjustable collimators upstream of Sirène; see Fig. 1 in Ref. [1].

TABLE I. Scintillation counter sizes and distances to the CH_2 target for the downstream polarimeter. For counter locations, see Fig. 1.

Counter	Height (mm)	Width (mm)	Thickness (mm)	Distance to target (cm)
PO1, PO5	50	40	15	60
PO2, PO6	60	60	5	120
PO3, PO7		85 mm dia.	5	18
PO4, PO8	150	60	5	46

The downstream polarimeter, shown schematically in Fig. 1, consisted of five arms with two or three scintillation counters apiece. Four arms were in the horizontal plane, similar to the SD3 polarimeter. Two arms were symmetrically located on opposite sides of the nominal beam line at laboratory angles $\sim 11.3°$, and included counter pairs PO_1 and PO_2, and PO_5 and PO_6. The manually adjusted recoil arms were approximately set at the angles corresponding to pp elastic-scattering kinematics, and contained counters PO_3 and PO_4, and PO_7 and PO_8. The fifth arm was located vertically and included VO_1, VO_2, and VO_3. The dimensions of the PO_j counters and their distances to the polarimeter target are given in Table I. Coincidences ($PO_1 \cdot PO_2 \cdot PO_3 \cdot PO_4$, $PO_5 \cdot PO_6 \cdot PO_7 \cdot PO_8$, and $VO_1 \cdot VO_2 \cdot VO_3$), and their respective accidentals were scaled.

The target was a block of CH_2 with dimensions 3.0 cm wide, 2.0 cm high, and 3.0 cm thick along the beam direction. It was smaller in width than the beam spot, which was typically several cm wide at this location.

The complete downstream polarimeter assembly was mounted on a remotely controlled table that could be moved horizontally, transverse to the beam. This was necessary be-

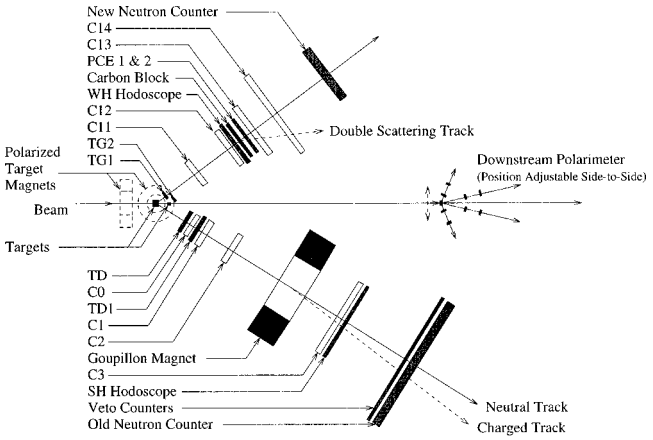

FIG. 2. Experimental layout showing the magnetic spectrometer and polarimeter arms and associated detectors (not to scale). The detectors are described in the text and Ref. [1].

TABLE II. Cross checks of the four relations $\mathcal{R}_k = 1$ from Eqs. (3) among the normalized elastic-scattering yields. The values of $\mathcal{R}_k$ are averages over all angles at each energy. The run period for each data set is also shown.

Energy (MeV)	$\mathcal{R}_1$	$\mathcal{R}_2$	$\mathcal{R}_3$	$\mathcal{R}_4$
795 IV	1.0113±0.0021	1.0061±0.0031	1.0027±0.0013	1.0046±0.0043
1975 III	1.0108±0.0060	1.0002±0.0069	0.9984±0.0020	1.0159±0.0112
2035 III	1.0075±0.0070	1.0057±0.0065	1.0006±0.0020	0.9934±0.0114
2035 IV	1.0060±0.0069	1.0135±0.0068	1.0040±0.0018	0.9941±0.0115
2115 III	0.9970±0.0057	1.0073±0.0077	1.0008±0.0021	0.9693±0.0110
2155 III	1.0059±0.0054	1.0033±0.0058	1.0006±0.0018	0.9948±0.0094
2175 III	0.9992±0.0071	1.0031±0.0056	0.9985±0.0017	0.9733±0.0107
2215 III	1.0069±0.0053	1.0059±0.0056	1.0013±0.0017	0.9866±0.0092
2225 IV	1.0166±0.0074	0.9976±0.0071	0.9993±0.0015	1.0194±0.0127
2235 III	1.0040±0.0059	1.0067±0.0073	1.0014±0.0021	0.9870±0.0112
2345 IV	0.9951±0.0077	0.9959±0.0079	0.9985±0.0018	0.9848±0.0133
2395 III	1.0068±0.0067	1.0119±0.0081	1.0023±0.0014	0.9912±0.0125
2445 IV	1.0133±0.0087	1.0013±0.0094	1.0012±0.0026	0.9918±0.0155
2495 III	1.0243±0.0089	1.0104±0.0094	1.0059±0.0027	1.0166±0.0158
2515 IV	1.0135±0.0092	0.9993±0.0082	1.0009±0.0022	1.0085±0.0150
2565 III	1.0070±0.0099	1.0218±0.0102	1.0055±0.0029	0.9665±0.0167
2575 IV	1.0065±0.0088	1.0008±0.0091	1.0013±0.0022	0.9745±0.0150
2595 III	1.0047±0.0066	1.0029±0.0094	1.0016±0.0024	0.9918±0.0137
2645 III	1.0096±0.0107	1.0179±0.0085	1.0047±0.0027	0.9834±0.0124
2795 IV	0.9920±0.0119	1.0299±0.0170	1.0016±0.0024	0.9144±0.0246

cause the magnetic field of the polarized target deflected the beam. However, it was also found that the beam position changed slightly with beam energy and beam tune when the polarized target magnet and spectrometer analyzing magnet (Goupillon) were turned off. This beam position was measured at most energies in run periods III and IV, and was found to change by ± 2.0 cm except at 795 MeV. It is estimated that this change corresponds to a variation in the incident beam angle at the polarized target of ± 3.1 mrad or less. At 795 MeV, the beam angle was found to be about 13 mrad from the nominal beam direction, and the data were corrected accordingly. This variation could cause a systematic error in the c.m. angle, and would appear as a zero crossing of $P = A_{oono}$ at an angle different from 90°; see Sec. III.

B. Polarized target and detectors

The polarized proton target used for these measurements is described in Refs. [1,6,7]. The size was $40(\mathrm{h}) \times 49(\mathrm{w}) \times 35(\mathrm{l})$ mm^3 and the target material was pentanol-3 ($CH_3CH_2CHOHCH_2CH_3$) in run period III and pentanol-2 ($CH_3CH_2CH_2CHOHCH_3$) in run period IV. The absolute target polarization was found by a comparison of the NMR signals in the polarized state and when the target material was in thermal equilibrium near 1 K. The thermal equilibrium calibrations were performed before and after each run period, and these calibrations agreed with each other within statistical errors. The target operated in the frozen-spin mode at a small magnetic holding field of 0.33 T. The typical target polarization magnitude was 0.65–0.85 before entering the frozen-spin mode.

The scattered and recoil protons were detected in coincidence. One detector arm consisted of a magnetic spectrometer, with five multiwire proportional chambers of 3–4 sense wire planes each, trigger scintillators, a scintillation counter hodoscope, and a set of neutron counters with associated charged particle veto counters. The other detector arm (polarimeter) consisted of two multiwire proportional chambers with three planes each, trigger scintillators, a scintillation counter hodoscope, plus other chambers and counters that were not used for the data described in this paper; see Fig. 2. Many additional details about the apparatus are given in Refs. [1,4,8,9]

In run period II, a new neutron counter hodoscope was installed in the polarimeter arm, and it became fully operational for run periods III and IV. The hodoscope detected protons and consisted of 11 bars of scintillator, each with cross sectional area $8(\mathrm{h}) \times 20(\mathrm{w})$ cm^2 and length 137 cm, with photomultipliers mounted on each end. Similar neutron counters are described in Ref. [11]. In addition, some changes to the associated electronics for both hodoscopes were made before run period III. However, the basic trigger conditions and quantities recorded for each event, namely pulse heights, flight times, and wire chamber information, were unchanged. The elastic-scattering A_N data were also generally in agreement; see Sec. IV.

III. DATA ANALYSIS

Details of the data analysis are presented in the accompanying paper, Ref. [1]. Values of scalers from each spill were

evaluated first to identify bad spills with anomalous run conditions. The polarimeter scalers were used to compute asymmetries and ratios to monitor the performance of the polarimeters and the beam polarization. This polarimeter information was used in the analysis of the elastic-scattering candidate events at a few energies, where the average beam polarization differed significantly for the two target-polarization-state time periods.

The elastic-scattering results were also tested for changes in the relative efficiency of hodoscope counters, wire chambers, or neutron counters. Histograms were generated of the number of times each wire was struck for each beam polarization state. Searches for sizable differences in these histograms were performed. Cuts were made to eliminate data from certain scintillation counters, individual wires, or wire chamber planes that exhibited evidence of variation in relative efficiency. Such variation could lead to systematic errors in the derived values of the spin observables. These cuts were applied for both target and all four beam polarization states.

After the cuts described above were made, the remaining elastic-scattering candidate events were analyzed. Particle positions were computed from the wire chamber signals. Straight lines were fitted to the positions in chambers C0, C1, C2 and in C11, C12. The observed laboratory angles were corrected for bending in the polarized target magnetic field to give (θ_L,ϕ_L) and (θ_R,ϕ_R) in the left and right detector arms, respectively. The two fitted lines were also projected to the target region, and the points at the distance of closest approach were obtained. The midpoint of the line segment connecting these two points was assigned to be the reconstructed interaction point. Events were rejected if (a) more than one counter was triggered in either hodoscope WH or SH, (b) the wire chamber data from three or four planes in C0 or three planes in any other chamber were not consistent with a single track in that chamber, or (c) there was insufficient information from the wire chambers to define the two lines or to calculate the momentum in the magnetic spectrometer arm. Cuts were also applied to (a) the reconstructed interaction point, (b) the difference in momentum between the value measured in the magnetic spectrometer arm and the calculated momentum from θ_R and elastic-scattering kinematics, and (c) the difference between the measured (and corrected) angle θ_R and the value computed from θ_L using elastic kinematics. The location of typical cuts are shown in Figs. 5 and 6 of Ref. [1].

Finally, the number of true elastic-scattering events at each angle was determined from the coplanarity distribution, $\Delta\phi=\phi_L+\phi_R-180°$, for each of the target and beam polarization states after estimating and subtracting remaining backgrounds. The number of elastic events was normalized to the relative beam intensity to give the quantities n_{ij}. Subscripts j and i correspond to the beam and target states, respectively. The normalized counts are expected to obey the relations

$$
\begin{aligned}
n_{+0+} &= C_0N[1+P_{0+}A_{oono}+P_{T+}A_{ooon}+P_{0+}P_{T+}A_{oonn}],\\
n_{+-} &= C_0N[1-P_{-}A_{oono}+P_{T+}A_{ooon}-P_{-}P_{T+}A_{oonn}],\\
n_{++} &= C_0N[1+P_{+}A_{oono}+P_{T+}A_{ooon}+P_{+}P_{T+}A_{oonn}],\\
n_{+0-} &= C_0N[1-P_{0-}A_{oono}+P_{T+}A_{ooon}-P_{0-}P_{T+}A_{oonn}],\\
n_{-0+} &= N[1+P_{0+}A_{oono}-P_{T-}A_{ooon}-P_{0+}P_{T-}A_{oonn}],\\
n_{--} &= N[1-P_{-}A_{oono}-P_{T-}A_{ooon}+P_{-}P_{T-}A_{oonn}],\\
n_{-+} &= N[1+P_{+}A_{oono}-P_{T-}A_{ooon}-P_{+}P_{T-}A_{oonn}],\\
n_{-0-} &= N[1-P_{0-}A_{oono}-P_{T-}A_{ooon}+P_{0-}P_{T-}A_{oonn}],
\end{aligned}
\tag{2}
$$

where P_j and P_{Ti} for the beam and target polarizations are expected to be positive values. It is assumed that there was only a slow variation in detector efficiencies over the period of beam polarization changes (seconds), but the equations allow for drifts in efficiencies with target polarization reversals (hours) via the factor C_0.

In Ref. [1], it is noted that four relations hold among the normalized counts, which can be expressed as ratios $\mathcal{R}_k$:

$$\mathcal{R}_1=\frac{n_{+0+}+n_{+0-}}{n_{++}+n_{+-}}=1, \tag{3a}$$

$$\mathcal{R}_2=\frac{n_{-0+}+n_{-0-}}{n_{-+}+n_{--}}=1, \tag{3b}$$

$$\mathcal{R}_3=\frac{n_{+0+}n_{--}+n_{+-}n_{-+}+n_{++}n_{-0+}}{n_{+-}n_{-0+}+n_{++}n_{--}+n_{+0+}n_{-+}}=1, \tag{3c}$$

$$\mathcal{R}_4=\frac{(0.072)n_{+-}n_{-+}+n_{+0+}n_{-+}+n_{+0+}n_{--}}{(0.072)n_{++}n_{--}+n_{++}n_{-0+}+n_{+-}n_{-0+}}=1. \tag{3d}$$

The factor 0.072 arises from the relative magnitudes of beam polarization states in Eq. (1). These ratios are computed as averages over all c.m. angles measured, and are shown in Table II. It can be seen that the results are generally consistent with $\mathcal{R}_k=1$, suggesting that certain systematic errors are small. For example, rapid changes in detector efficiencies would generally result in $\mathcal{R}_k\neq 1$ at an energy.

Equations (2) were solved for the spin observable $A_{oon}=P=A_N$ at each c.m. angle as described in Ref. [1]. Two independent analyses were performed, with slightly different cuts, and the results were combined for this paper. They are given in Table III and Figs. 3–8. Relative and additive errors, $\sigma_{\rm rel}$ and $\sigma_{\rm add}$, respectively, are also shown. The total error on A_{oon} is given by

TABLE III. (a) Measured values of the analyzing power A_{oon} at $T=795$ MeV. The quantities $\langle\theta_{\text{c.m.}}\rangle$ and $-t$ are the central values of the c.m. angle and four-momentum transfer squared for each bin in degrees and $(\text{GeV}/c)^2$, respectively. The relative and additive systematic errors are ±0.018 and ±0.0007, respectively. (b) Measured values of A_{oon} at $T=1975$ MeV. The relative and additive systematic errors are ±0.045 and ±0.002, respectively. (c) Measured values of A_{oon} at 2035 MeV in run period III. The relative and additive systematic errors are ±0.044 and ±0.002, respectively. (d) Measured values of A_{oon} at $T=2035$ MeV in run period IV. The relative and additive systematic errors are ±0.050 and ±0.001, respectively. (e) Measured values of A_{oon} at 2115 MeV. The relative and additive systematic errors are ±0.038 and ±0.001, respectively. (f) Measured values of A_{oon} at 2155 MeV. The relative and additive systematic errors are ±0.030 and ±0.001, respectively. (g) Measured values of A_{oon} at 2175 MeV. The relative and additive systematic errors are ±0.032 and ±0.001, respectively. (h) Measured values of A_{oon} at 2215 MeV. The relative and additive systematic errors are ±0.028 and ±0.001, respectively. (i) Measured values of A_{oon} at 2225 MeV. The relative and additive systematic errors are ±0.042 and ±0.001, respectively. (j) Measured values of A_{oon} at 2235 MeV. The relative and additive systematic errors are ±0.034 and ±0.001, respectively. (k) Measured values of A_{oon} at 2345 MeV. The relative and additive systematic errors are ±0.040 and ±0.001, respectively. (l) Measured values of A_{oon} at 2395 MeV. The relative and additive systematic errors are ±0.039 and ±0.002, respectively. (m) Measured values of A_{oon} at 2445 MeV. The relative and additive systematic errors are ±0.042 and ±0.001, respectively. (n) Measured values of A_{oon} at 2495 MeV. The relative and additive systematic errors are ±0.034 and ±0.002, respectively. (o) Measured values of A_{oon} at 2515 MeV. The relative and additive systematic errors are ±0.036 and ±0.001, respectively. (p) Measured values of A_{oon} at 2565 MeV. The relative and additive systematic errors are ±0.036 and ±0.001, respectively. (q) Measured values of A_{oon} at 2575 MeV. The relative and additive systematic errors are ±0.035 and ±0.001, respectively. (r) Measured values of A_{oon} at 2595 MeV. The relative and additive systematic errors are ±0.034 and ±0.001, respectively. (s) Measured values of A_{oon} at 2645 MeV. The relative and additive systematic errors are ±0.035 and ±0.001, respectively. (t) Measured values of A_{oon} at 2795 MeV. The relative and additive systematic errors are ±0.061 and ±0.001, respectively.

$\langle\theta_{\text{c.m.}}\rangle$	$-t$	A_{oon}	ΔA_{oon}	$\langle\theta_{\text{c.m.}}\rangle$	$-t$	A_{oon}	ΔA_{oon}
	(a) 795 MeV			80.0	0.617	0.2174	0.0068
47.4	0.241	0.4851	0.0150	81.0	0.630	0.1986	0.0060
48.2	0.249	0.4941	0.0055	82.0	0.642	0.1788	0.0127
49.2	0.258	0.4924	0.0061	83.0	0.655	0.1560	0.0074
50.2	0.269	0.4921	0.0057	84.0	0.668	0.1322	0.0064
51.1	0.278	0.4850	0.0066	85.0	0.681	0.1043	0.0136
52.1	0.288	0.4813	0.0104	86.0	0.694	0.1006	0.0071
53.1	0.298	0.4805	0.0147	87.0	0.707	0.0682	0.0084
54.2	0.309	0.4742	0.0052	88.0	0.720	0.0468	0.0058
55.1	0.320	0.4660	0.0070	88.8	0.731	0.0146	0.0123
56.2	0.331	0.4574	0.0119	89.7	0.742	0.0076	0.0275
57.1	0.341	0.4657	0.0045		(b) 1975 MeV		
58.1	0.352	0.4534	0.0073	60.5	0.940	0.117	0.019
59.1	0.363	0.4466	0.0047	62.0	0.983	0.128	0.015
60.1	0.374	0.4590	0.0046	64.0	1.041	0.107	0.010
61.1	0.385	0.4400	0.0058	65.9	1.097	0.101	0.011
62.1	0.397	0.4329	0.0046	68.0	1.160	0.100	0.017
63.1	0.409	0.4225	0.0050	70.0	1.219	0.130	0.012
64.1	0.420	0.4156	0.0082	72.0	1.280	0.107	0.015
65.1	0.432	0.4135	0.0060	74.0	1.342	0.133	0.016
66.0	0.443	0.4040	0.0060	76.0	1.406	0.113	0.014
67.1	0.455	0.4058	0.0052	77.9	1.466	0.078	0.012
68.1	0.467	0.3833	0.0078	80.0	1.533	0.063	0.012
69.1	0.479	0.3699	0.0055	82.0	1.595	0.042	0.011
70.1	0.491	0.3571	0.0075	84.0	1.659	0.056	0.022
71.0	0.504	0.3490	0.0052	86.0	1.725	0.042	0.013
72.1	0.517	0.3422	0.0063	88.0	1.789	0.014	0.013
73.1	0.529	0.3226	0.0059	89.9	1.851	0.006	0.018
74.0	0.541	0.3162	0.0050	92.0	1.919	−0.024	0.014
75.1	0.554	0.2993	0.0067	94.0	1.982	−0.030	0.020
76.0	0.566	0.2878	0.0072	96.0	2.046	−0.061	0.022
77.1	0.579	0.2673	0.0059	98.0	2.110	−0.060	0.012
78.0	0.591	0.2431	0.0086	99.9	2.171	−0.094	0.012
79.0	0.604	0.2462	0.0068	101.2	2.213	−0.206	0.098

TABLE III. (*Continued*).

$\langle\theta_{\text{c.m.}}\rangle$	$-t$	A_{oon}	ΔA_{oon}
	(c) 2035 MeV		
60.2	0.962	0.105	0.012
62.0	1.013	0.121	0.012
64.0	1.072	0.105	0.015
65.9	1.130	0.129	0.012
68.1	1.197	0.124	0.011
70.0	1.256	0.123	0.012
72.0	1.319	0.123	0.012
74.0	1.383	0.108	0.013
76.0	1.447	0.097	0.011
78.0	1.512	0.087	0.011
79.4	1.558	0.050	0.022
82.0	1.647	0.052	0.018
84.0	1.710	0.047	0.012
86.0	1.776	0.031	0.013
88.0	1.844	0.002	0.011
90.0	1.909	−0.010	0.012
92.1	1.979	−0.053	0.012
94.0	2.042	−0.074	0.018
96.0	2.109	−0.047	0.030
98.0	2.175	−0.081	0.023
99.9	2.238	−0.072	0.014
101.3	2.283	−0.054	0.053
	(d) 2035 MeV		
60.3	0.964	0.120	0.011
62.0	1.013	0.128	0.009
64.0	1.072	0.123	0.009
66.0	1.133	0.123	0.010
67.5	1.179	0.177	0.016
72.0	1.319	0.129	0.020
74.0	1.383	0.114	0.010
76.0	1.447	0.096	0.014
78.0	1.512	0.085	0.012
80.0	1.578	0.067	0.012
82.0	1.643	0.049	0.013
84.0	1.710	0.034	0.012
86.0	1.776	0.020	0.021
88.0	1.844	0.000	0.011
90.0	1.909	−0.015	0.011
92.0	1.977	−0.034	0.011
94.0	2.042	−0.036	0.020
96.0	2.109	−0.080	0.013
98.0	2.175	−0.077	0.016
100.0	2.241	−0.102	0.018
101.3	2.283	−0.091	0.027
	(e) 2115 MeV		
58.8	0.953	0.090	0.046
60.1	0.995	0.127	0.010
62.0	1.052	0.131	0.010
64.0	1.115	0.146	0.011
66.0	1.176	0.156	0.016
68.0	1.243	0.141	0.011
70.0	1.306	0.133	0.011
72.0	1.371	0.137	0.012
74.0	1.437	0.120	0.012
76.0	1.504	0.126	0.011
78.0	1.572	0.115	0.014
80.0	1.640	0.098	0.014
82.0	1.709	0.079	0.012
83.9	1.774	0.080	0.012
88.1	1.917	0.047	0.012
90.0	1.983	−0.014	0.012
92.0	2.054	−0.028	0.012
94.0	2.123	−0.072	0.016
96.0	2.192	−0.085	0.017
97.9	2.259	−0.092	0.012
99.9	2.327	−0.124	0.013
101.5	2.381	−0.117	0.017
	(f) 2155 MeV		
58.7	0.973	0.170	0.028
60.1	1.013	0.155	0.010
62.0	1.073	0.154	0.010
64.0	1.136	0.170	0.009
66.0	1.199	0.161	0.012
68.0	1.265	0.166	0.012
70.0	1.330	0.176	0.009
72.0	1.397	0.144	0.008
74.0	1.465	0.149	0.010
76.0	1.533	0.126	0.014
78.0	1.602	0.135	0.016
80.5	1.688	0.070	0.016
82.0	1.742	0.077	0.014
83.9	1.808	0.073	0.012
86.0	1.881	0.032	0.012
88.1	1.955	0.020	0.010
90.0	2.021	−0.004	0.014
92.0	2.092	−0.056	0.010
94.0	2.163	−0.060	0.012
96.0	2.233	−0.081	0.012
98.0	2.302	−0.084	0.014
99.9	2.371	−0.123	0.010
101.7	2.431	−0.151	0.017
	(g) 2175 MeV		
58.7	0.982	0.133	0.023
60.0	1.021	0.160	0.009
62.0	1.083	0.153	0.012
64.0	1.146	0.149	0.010
66.0	1.211	0.177	0.010
68.0	1.276	0.161	0.013
70.0	1.343	0.146	0.014
72.0	1.410	0.150	0.010
74.0	1.479	0.134	0.011
76.0	1.547	0.126	0.010
78.0	1.616	0.118	0.011
80.0	1.686	0.111	0.011
82.0	1.758	0.036	0.012
84.0	1.827	0.064	0.011
86.0	1.899	0.038	0.014

TABLE III. (*Continued*).

$\langle\theta_{\text{c.m.}}\rangle$	$-t$	A_{oon}	ΔA_{oon}	$\langle\theta_{\text{c.m.}}\rangle$	$-t$	A_{oon}	ΔA_{oon}
88.1	1.972	0.012	0.012	100.0	2.451	−0.140	0.026
90.0	2.041	−0.026	0.012	101.9	2.520	−0.163	0.037
92.0	2.111	−0.044	0.011	103.2	2.563	−0.101	0.062
94.0	2.183	−0.058	0.013	(j) 2235 MeV			
96.0	2.254	−0.075	0.012	58.8	1.010	0.155	0.020
98.0	2.324	−0.100	0.011	60.0	1.048	0.167	0.010
100.0	2.394	−0.108	0.014	62.0	1.113	0.192	0.010
101.7	2.456	−0.124	0.013	64.0	1.178	0.186	0.010
(h) 2215 MeV				66.0	1.244	0.184	0.013
58.7	1.000	0.145	0.018	68.0	1.310	0.190	0.010
60.0	1.040	0.169	0.008	70.0	1.380	0.181	0.010
62.0	1.103	0.174	0.008	72.0	1.449	0.157	0.011
64.0	1.167	0.183	0.008	74.0	1.520	0.150	0.011
66.5	1.250	0.167	0.012	76.0	1.590	0.148	0.011
68.0	1.299	0.177	0.009	78.0	1.661	0.120	0.011
70.0	1.367	0.167	0.009	80.0	1.733	0.093	0.012
72.0	1.436	0.152	0.008	82.1	1.807	0.079	0.011
74.0	1.505	0.138	0.009	84.0	1.878	0.049	0.012
76.0	1.575	0.159	0.009	86.0	1.951	0.042	0.013
78.0	1.646	0.130	0.009	88.0	2.024	−0.003	0.011
80.0	1.717	0.114	0.010	90.0	2.097	−0.022	0.012
82.1	1.793	0.088	0.010	92.0	2.169	−0.031	0.012
84.0	1.861	0.073	0.009	94.0	2.244	−0.068	0.014
86.0	1.934	0.032	0.009	96.0	2.316	−0.093	0.013
88.0	2.006	0.027	0.009	98.0	2.388	−0.097	0.012
90.0	2.078	−0.014	0.011	100.0	2.460	−0.133	0.012
92.0	2.150	−0.039	0.010	101.9	2.529	−0.136	0.012
94.0	2.223	−0.065	0.010	103.2	2.575	−0.178	0.080
96.0	2.296	−0.092	0.011	(k) 2345 MeV			
98.0	2.366	−0.100	0.012	58.0	1.035	0.177	0.037
100.0	2.438	−0.111	0.010	60.0	1.101	0.173	0.012
101.8	2.504	−0.145	0.012	62.0	1.168	0.186	0.013
(i) 2225 MeV				64.0	1.235	0.182	0.016
58.7	1.003	0.194	0.025	66.0	1.306	0.163	0.016
60.0	1.044	0.142	0.010	68.5	1.393	0.183	0.017
62.0	1.108	0.146	0.010	69.8	1.442	0.149	0.020
64.0	1.172	0.146	0.010	72.0	1.520	0.106	0.022
66.0	1.239	0.147	0.012	74.2	1.601	0.153	0.015
67.9	1.303	0.151	0.012	76.0	1.667	0.170	0.014
70.0	1.374	0.147	0.016	78.0	1.743	0.149	0.014
72.0	1.444	0.143	0.015	80.5	1.837	0.111	0.019
74.0	1.512	0.128	0.020	82.0	1.894	0.105	0.015
76.0	1.583	0.102	0.022	84.0	1.971	0.068	0.014
78.0	1.654	0.102	0.012	86.0	2.046	0.070	0.017
80.0	1.725	0.083	0.012	88.0	2.123	0.022	0.017
82.1	1.800	0.060	0.013	90.0	2.201	−0.021	0.015
84.0	1.869	0.021	0.023	92.0	2.276	−0.019	0.015
86.0	1.942	0.041	0.020	94.0	2.354	−0.039	0.020
88.0	2.014	0.005	0.014	96.0	2.430	−0.050	0.017
90.0	2.088	−0.024	0.013	98.0	2.506	−0.111	0.015
92.0	2.160	−0.051	0.016	100.0	2.583	−0.142	0.015
94.0	2.233	−0.099	0.015	102.0	2.658	−0.163	0.020
96.0	2.306	−0.116	0.029	103.5	2.716	−0.185	0.025
98.0	2.378	−0.119	0.023				

TABLE III. (*Continued*).

$\langle\theta_{\text{c.m.}}\rangle$	$-t$	A_{oon}	ΔA_{oon}
	(l) 2395 MeV		
60.2	1.129	0.187	0.016
62.0	1.192	0.180	0.013
64.0	1.261	0.186	0.022
66.0	1.334	0.196	0.014
68.0	1.405	0.197	0.013
70.1	1.481	0.179	0.019
72.0	1.552	0.177	0.023
74.0	1.628	0.180	0.019
76.0	1.702	0.155	0.014
78.0	1.780	0.130	0.018
80.0	1.856	0.125	0.016
81.9	1.932	0.102	0.019
84.0	2.012	0.068	0.019
86.0	2.089	0.049	0.017
88.0	2.168	0.001	0.020
90.0	2.248	−0.026	0.017
92.0	2.326	−0.051	0.017
94.0	2.403	−0.054	0.019
96.0	2.482	−0.105	0.019
98.0	2.560	−0.119	0.023
100.0	2.637	−0.123	0.016
102.0	2.714	−0.170	0.021
103.7	2.778	−0.189	0.023
	(m) 2445 MeV		
59.7	1.137	0.230	0.029
62.0	1.217	0.187	0.013
63.9	1.287	0.188	0.013
66.0	1.362	0.196	0.014
68.0	1.434	0.168	0.014
69.9	1.504	0.220	0.016
72.0	1.585	0.214	0.027
74.1	1.667	0.198	0.021
76.0	1.738	0.158	0.019
78.0	1.817	0.132	0.020
80.0	1.896	0.112	0.017
82.0	1.973	0.099	0.018
84.0	2.056	0.068	0.016
86.0	2.134	0.067	0.026
88.0	2.213	−0.010	0.025
90.0	2.295	−0.011	0.029
92.5	2.394	−0.055	0.026
94.0	2.455	−0.091	0.016
96.0	2.534	−0.107	0.017
98.0	2.614	−0.153	0.021
100.0	2.692	−0.163	0.018
102.0	2.771	−0.157	0.035
103.9	2.844	−0.202	0.018
	(n) 2495 MeV		
60.5	1.187	0.202	0.017
62.0	1.242	0.203	0.013
64.0	1.313	0.218	0.014
66.0	1.389	0.223	0.015
68.0	1.464	0.229	0.015
70.0	1.539	0.237	0.014
72.0	1.618	0.211	0.014
74.0	1.696	0.207	0.014
76.0	1.773	0.195	0.018
78.0	1.856	0.160	0.015
80.0	1.935	0.157	0.016
82.0	2.015	0.123	0.016
84.1	2.099	0.058	0.017
86.0	2.178	0.064	0.020
88.0	2.258	0.052	0.017
90.0	2.342	0.003	0.017
92.0	2.423	−0.034	0.017
94.0	2.503	−0.047	0.016
96.1	2.588	−0.102	0.016
98.0	2.668	−0.089	0.017
100.0	2.748	−0.107	0.016
102.0	2.828	−0.180	0.016
103.9	2.905	−0.213	0.017
105.2	2.953	−0.393	0.088
	(o) 2515 MeV		
60.6	1.200	0.224	0.017
62.0	1.252	0.194	0.011
64.0	1.324	0.203	0.012
66.0	1.400	0.226	0.012
68.0	1.475	0.204	0.012
69.9	1.549	0.225	0.016
71.9	1.628	0.199	0.023
74.0	1.710	0.186	0.026
76.1	1.791	0.175	0.015
78.0	1.869	0.172	0.016
80.0	1.950	0.134	0.014
82.0	2.031	0.143	0.015
84.0	2.115	0.099	0.014
86.0	2.195	0.063	0.014
88.0	2.276	0.025	0.016
90.0	2.360	0.018	0.022
92.0	2.442	−0.015	0.017
94.0	2.524	−0.038	0.018
96.0	2.607	−0.072	0.016
98.0	2.689	−0.098	0.019
100.0	2.770	−0.135	0.018
102.0	2.851	−0.133	0.015
104.0	2.929	−0.161	0.017
105.2	2.979	−0.208	0.045
	(p) 2565 MeV		
60.7	1.228	0.175	0.031
62.0	1.277	0.216	0.019
64.0	1.350	0.198	0.014
66.0	1.427	0.219	0.014
68.0	1.505	0.216	0.019
69.9	1.580	0.218	0.019
72.1	1.665	0.196	0.020
74.0	1.743	0.190	0.016

TABLE III. (*Continued*).

$\langle\theta_{\text{c.m.}}\rangle$	$-t$	A_{oon}	ΔA_{oon}	$\langle\theta_{\text{c.m.}}\rangle$	$-t$	A_{oon}	ΔA_{oon}
76.0	1.823	0.167	0.015	84.0	2.180	0.091	0.016
78.0	1.908	0.162	0.018	86.0	2.265	0.073	0.013
80.0	1.989	0.141	0.015	88.0	2.349	0.050	0.015
82.0	2.071	0.097	0.016	90.0	2.434	−0.019	0.016
84.0	2.156	0.102	0.017	92.0	2.521	−0.053	0.016
86.0	2.239	0.087	0.018	94.0	2.605	−0.085	0.014
88.0	2.322	0.026	0.018	96.0	2.689	−0.115	0.015
90.0	2.407	0.008	0.023	98.0	2.774	−0.131	0.014
92.0	2.490	−0.025	0.020	100.0	2.857	−0.151	0.017
94.0	2.575	−0.072	0.023	102.0	2.941	−0.181	0.014
96.0	2.659	−0.058	0.027	104.0	3.024	−0.193	0.013
98.1	2.744	−0.092	0.026	105.4	3.081	−0.190	0.023
100.0	2.825	−0.136	0.017	(s) 2645 MeV			
102.0	2.907	−0.200	0.019	60.7	1.268	0.291	0.065
104.0	2.990	−0.177	0.016	62.0	1.318	0.198	0.014
105.3	3.043	−0.221	0.038	64.0	1.395	0.241	0.016
(q) 2575 MeV				66.0	1.472	0.217	0.014
60.7	1.233	0.186	0.022	68.0	1.551	0.257	0.017
62.0	1.281	0.179	0.013	69.9	1.631	0.237	0.015
64.0	1.356	0.225	0.014	72.1	1.719	0.196	0.014
66.0	1.434	0.204	0.019	74.0	1.797	0.201	0.019
68.0	1.511	0.193	0.018	76.0	1.881	0.183	0.016
69.9	1.587	0.193	0.014	78.0	1.964	0.158	0.018
71.4	1.646	0.245	0.028	80.0	2.052	0.142	0.016
74.5	1.771	0.237	0.033	82.0	2.135	0.098	0.024
76.5	1.852	0.151	0.023	83.9	2.220	0.066	0.018
78.0	1.913	0.151	0.014	86.0	2.308	0.075	0.017
80.0	1.997	0.120	0.023	88.0	2.396	0.021	0.020
82.0	2.079	0.104	0.015	90.0	2.482	0.034	0.022
84.0	2.164	0.074	0.019	92.0	2.570	−0.033	0.019
86.0	2.247	0.056	0.018	94.0	2.654	−0.112	0.020
88.0	2.331	0.007	0.018	96.0	2.740	−0.087	0.018
90.0	2.416	−0.045	0.026	98.0	2.828	−0.129	0.017
92.0	2.501	−0.041	0.022	100.0	2.913	−0.111	0.023
94.0	2.585	−0.101	0.016	102.0	2.997	−0.158	0.017
96.0	2.668	−0.086	0.020	104.0	3.082	−0.200	0.016
98.0	2.753	−0.147	0.018	105.3	3.137	−0.186	0.035
100.0	2.836	−0.169	0.022	(t) 2795 MeV			
102.0	2.918	−0.210	0.015	62.9	1.428	0.125	0.026
104.0	3.000	−0.194	0.015	65.5	1.535	0.160	0.019
105.3	3.054	−0.196	0.036	68.5	1.661	0.131	0.020
(r) 2595 MeV				71.4	1.786	0.149	0.028
60.7	1.243	0.236	0.024	74.4	1.917	0.135	0.034
62.0	1.291	0.198	0.010	77.8	2.070	0.119	0.032
64.0	1.367	0.192	0.012	80.5	2.189	0.072	0.020
66.0	1.444	0.203	0.013	83.4	2.323	0.112	0.019
68.0	1.522	0.187	0.012	86.5	2.465	0.007	0.032
69.9	1.599	0.187	0.015	89.4	2.596	0.017	0.030
72.1	1.685	0.186	0.013	92.5	2.738	−0.096	0.033
74.0	1.763	0.166	0.014	95.5	2.873	−0.074	0.021
76.0	1.844	0.182	0.013	98.5	3.011	−0.112	0.022
78.0	1.929	0.164	0.015	101.6	3.148	−0.174	0.034
80.0	2.013	0.162	0.017	104.1	3.263	−0.173	0.023
82.0	2.095	0.124	0.021				

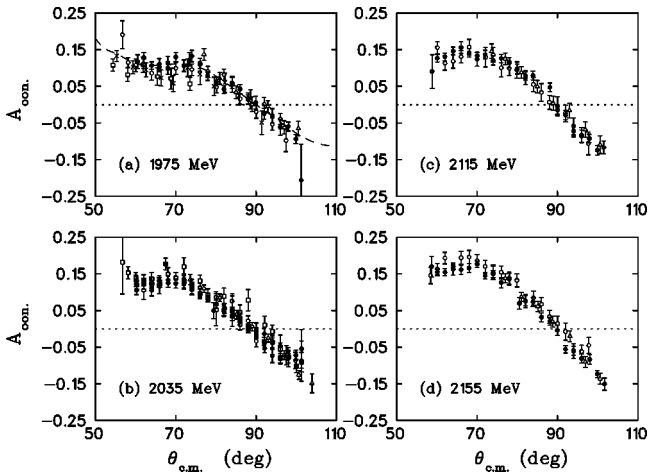

FIG. 3. Experimental results for $A_{oon}=A_N$ as a function of c.m. angle at 1975, 2035, 2115, and 2155 MeV. The closed circles and closed squares are from this paper, the open circles and open squares from Ref. [1], and the open triangles from Ref. [2]. The crosses are data from Parry *et al.* [13], and the dashed line is from a PSA prediction of Arndt *et al.* [30].

$$(\delta A_{oon})^2=(\delta A_{oon,\mathrm{stat}})^2+(A_{oon}\times\sigma_{\mathrm{rel}})^2+(\sigma_{\mathrm{add}})^2, \quad (4)$$

where $\delta A_{oon,\mathrm{stat}}$ is the statistical uncertainty.

The value $A_N(90°)$ should be zero for pp elastic scattering by the generalized Pauli principle [12]. The measured values for $\theta_{\mathrm{c.m.}}=90\pm5°$ were fit with a straight line to yield the result at 90° as well as the slope. These are presented in Table IV and Fig. 9. Data from Ref. [1] are also plotted. The $A_{oon}(90°)$ results are seen to be consistent with a slightly negative value, probably caused by a slight misalignment of the apparatus compared to the actual average beam direction. Variations in $A_{oon}(90°)$, possibly the result of small changes in the beam direction or other systematic errors, are smaller than ±0.03.

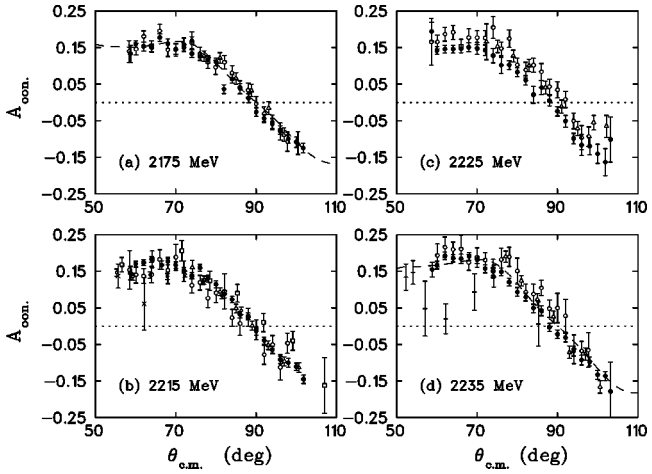

FIG. 4. Experimental results for $A_{oon}=A_N$ as a function of c.m. angle at 2175, 2215, 2225, and 2235 MeV. The closed circles are from this paper, the open circles from Ref. [1], and the open triangles from Ref. [2]. In addition, the open squares are from Miller *et al.* [14], the pluses from Neal and Longo [15], the crosses from Diebold *et al.* [17], and the open diamonds from Makdisi *et al.* [18]. The dashed curves are from PSA predictions of Arndt *et al.* [30].

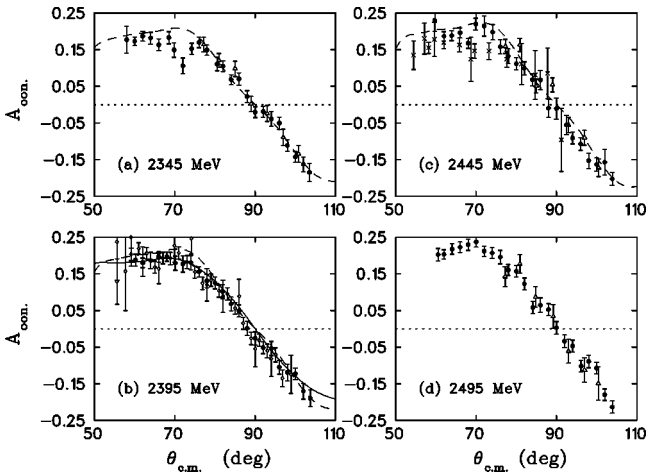

FIG. 5. Experimental results for $A_{oon}=A_N$ as a function of c.m. angle at 2345, 2395, 2445, and 2495 MeV. The closed circles are from this paper, and the open triangles from Ref. [2]. The open diamonds are data from Perrot *et al.* [16], and the crosses from Parry *et al.* [13]. The solid curve is from a PSA prediction of the Saclay-Geneva group [21] and the dashed curves from Arndt *et al.* [30].

IV. RESULTS

A comparison of the data from this paper and the accompanying article [1] is shown in Figs. 3 and 4. The A_{oono} measurements performed simultaneously, using a CH_2 target [2], are also included in Figs. 3–7. The same beam polarizations were used for the A_{oon} data from the polarized target and for the A_{oono} results from the CH_2 target. The agreement is generally very good except near 2225 MeV.

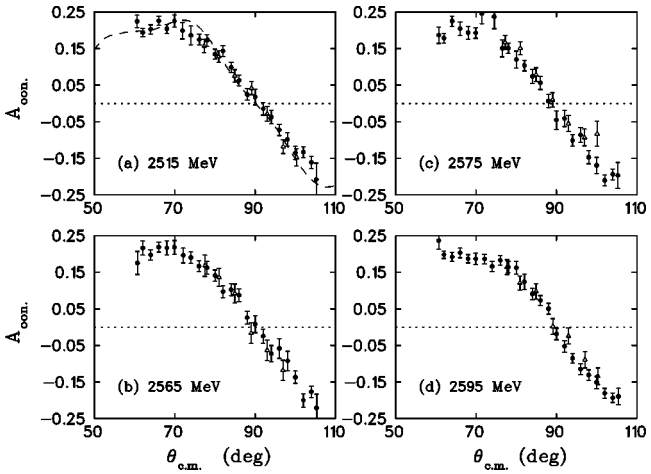

FIG. 6. Experimental results for $A_{oon}=A_N$ as a function of c.m. angle at 2515, 2565, 2575, and 2595 MeV. The closed circles are from this paper, and the open triangles from Ref. [2]. The dashed curve is from a PSA prediction of Arndt *et al.* [30].

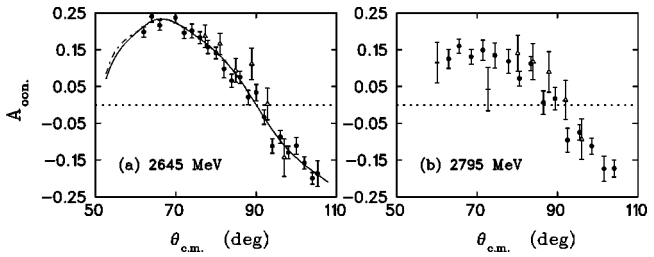

FIG. 7. Experimental results for $A_{oon}=A_N$ as a function of c.m. angle at 2645 and 2795 MeV. The closed circles are from this paper, the open triangles from Ref. [2], and the pluses from Neal and Longo [15]. The solid and dot-dashed curves are from PSA predictions of the Saclay-Geneva group [21].

Data at 2205, 2215, 2225, and 2235 MeV from Ref. [1] were collected in run period I. For these four data sets, the proton beam was accelerated to 2240 MeV, and absorbers were used to degrade the energy for the three lower energies. This was done so that the beam would be accelerated to a value well above a strong depolarizing resonance at 2201 MeV in Saturne II. The results in this paper at 2215 and 2235 MeV were collected in run period III, and at 2225 MeV in run period IV; none of these data used a degrader in the beam. The results from run period I are seen to be slightly below the new data at 2215 MeV, and somewhat above at 2225 and 2235 MeV. Careful searches of the data for changes in efficiency or other possible systematic errors have been performed, but none were found. It is believed that the beam polarization, P_B, for the 2225 MeV data in this paper is too large by about three standard deviations, possibly caused by a statistical fluctuation and the method used to determine P_B from the measurements; see Ref. [1]. A correction to P_B would raise the A_{oon} values from run period IV to be in better agreement with those from run period I.

Previous results are also shown in Figs. 3–5, 7. The data of Parry *et al.* [13] at 1967 and 2444 MeV exhibit good agreement over part of the angular range, but appear somewhat low near 70° c.m. Similarly, the results of Miller *et al.* [14] at 2205 MeV may be a bit high at large angles, but agree over the rest of the angular range. The data of Neal and Longo [15] at 2240 MeV appear considerably low, but do not disagree as badly at 2840 MeV. The 2393–2396 MeV results of Perrot *et al.* [16] and the 2205 MeV measurements of Makdisi *et al.* [18] agree very well with the results in this paper. The two points of Diebold *et al.* [17] at 2205 MeV are also shown at small angles. Some time ago, a study of the Zero-Gradient Synchrotron beam polarization was performed [19]. A global analysis of pp analyzing power data at small angles ($|t|\leqslant 0.7$ GeV$^2/c^2$) was included, and as a byproduct it was concluded that the data of Refs. [13,17] should be renormalized upward by 15% and 10%, respectively, while no changes were suggested for Refs. [14,15]. The suggested changes would improve the agreement with the new data from this paper.

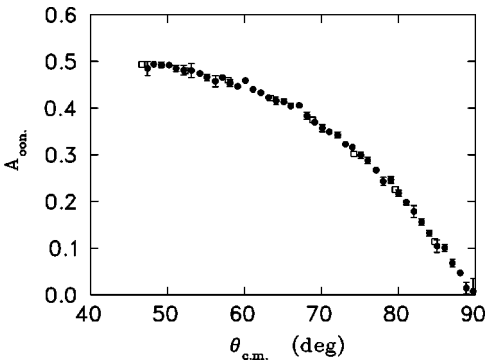

FIG. 8. Experimental results for $A_{oon}=A_N$ as a function of c.m. angle at 795 MeV compared to Lampf data of Bevington *et al.* [20]. The closed circles are from this paper and the open squares from Ref. [20].

TABLE IV. Results from straight line fits to the A_{oon} data near 90° c.m. The beam kinetic energy, fitted slope, angle at zero crossing, and value at 90° are all presented. The 90° data include systematic errors. The values of χ^2 per degree of freedom for the weighted averages are 2.26 and 2.21, respectively.

Energy (MeV)	Slope (deg^{-1})	Angle (deg.)	$A_{oon}(90°)$
1975	-0.0095 ± 0.0024	90.00 ± 0.72	0.0000 ± 0.0071
2035 III	-0.0131 ± 0.0022	88.46 ± 0.47	-0.0202 ± 0.0061
2035 IV	-0.0077 ± 0.0027	88.05 ± 1.01	-0.0151 ± 0.0059
2115	-0.0189 ± 0.0031	90.13 ± 0.35	0.0024 ± 0.0068
2155	-0.0135 ± 0.0019	88.94 ± 0.41	-0.0143 ± 0.0052
2175	-0.0125 ± 0.0021	88.72 ± 0.50	-0.0160 ± 0.0058
2215	-0.0129 ± 0.0015	89.11 ± 0.34	-0.0115 ± 0.0044
2225	-0.0169 ± 0.0026	88.46 ± 0.49	-0.0260 ± 0.0069
2235	-0.0121 ± 0.0021	88.58 ± 0.51	-0.0171 ± 0.0057
2345	-0.0132 ± 0.0028	90.09 ± 0.55	0.0012 ± 0.0074
2395	-0.0134 ± 0.0028	88.78 ± 0.64	-0.0163 ± 0.0081
2445	-0.0176 ± 0.0033	88.91 ± 0.70	-0.0192 ± 0.0109
2495	-0.0156 ± 0.0028	90.54 ± 0.50	0.0084 ± 0.0079
2515	-0.0121 ± 0.0026	90.82 ± 0.69	0.0100 ± 0.0078
2565	-0.0184 ± 0.0031	90.24 ± 0.49	0.0044 ± 0.0090
2575	-0.0185 ± 0.0027	88.69 ± 0.50	-0.0242 ± 0.0085
2595	-0.0208 ± 0.0022	89.70 ± 0.31	-0.0062 ± 0.0066
2645	-0.0213 ± 0.0029	89.77 ± 0.40	-0.0049 ± 0.0087
2795	-0.0110 ± 0.0039	88.01 ± 1.92	-0.0218 ± 0.0160
Wt. Av.		89.39 ± 0.11	-0.0104 ± 0.0016

Knowledge of the absolute target polarization is one of the largest contributions to the systematic error on the A_{oon} results. Data were collected at 795 MeV during run period IV in order to check the absolute target polarization with respect to the known beam polarization. These are compared with the very precise LAMPF measurements of Bevington *et al.* [20] in Fig. 8; very good agreement is seen. A weighted average of the ratio of the two data sets as a function of $\theta_{c.m.}$ gives

$$\left\langle \frac{A_N(\text{Saclay})}{A_N(\text{LAMPF})} \right\rangle = 1.002\pm0.008,$$

where only the statistical error is quoted. A careful comparison of our 795 MeV data and the results of Bevington *et al.*

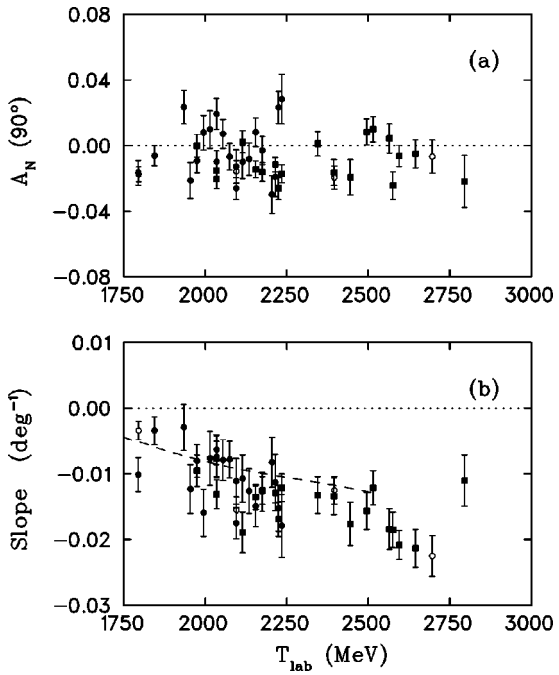

FIG. 9. Plots of (a) $A_N(90°)$ and (b) the slope $dA_N/d\theta$ at 90° c.m. as a function of beam kinetic energy. These values were computed from data between 85–95°. The solid circles are from Ref. [1], the solid squares from this paper, and the open circles from Perrot *et al.* [16]. The dashed curve is from a PSA prediction of Arndt *et al.* [30].

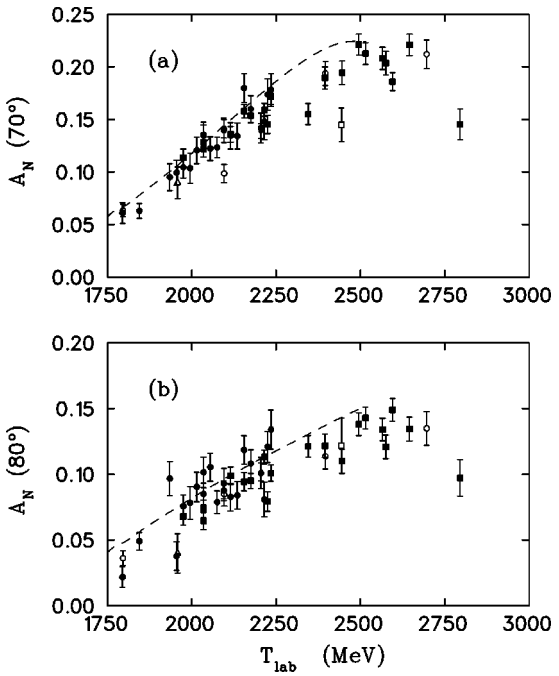

FIG. 10. Experimental results for A_N at (a) 70° and (b) 80° c.m. taken from averages over 65–75° and 75–85°. The solid squares are from this paper, the solid circles from Ref. [1], the open circles from Perrot *et al.* [16], the open triangles from Albrow *et al.* [22], the open squares from Parry *et al.* [13], and the open diamonds from Makdisi *et al.* [18]. The dashed curves are from PSA predictions of Arndt *et al.* [30].

was performed with the Saclay-Geneva fixed energy phase-shift analysis (PSA) (Ref. [21], 795 MeV solution, unpublished). An upper limit to a possible systematic difference between the different data sets was found to be 0.9%. The data are in full statistical agreement, and the distribution of the values with respect to the common fit agrees with the expected χ-squared distribution. It is concluded that the normalizations of the Saclay and LAMPF data agree within statistical uncertainties. Other measurements close to this energy and in the angular range of the results in this paper are given in Refs. [22,23], but the statistical uncertainties are much larger than in Bevington *et al.* [20].

A search was performed for rapid energy dependence in A_N. Data from Ref. [1] and this paper were averaged over the c.m. angular ranges 65–75° and 75–85° and are shown in Fig. 10. Similarly, the slopes at 90°, $dA_N/d\theta$, are given in Fig. 9(b). Data from Perrot *et al.* [16] at 1796, 2096, 2396, and 2696 MeV, from Albrow *et al.* [22] at 1958 MeV, from Parry *et al.* [13] at 2444 MeV, and from Makdisi *et al.* [18] at 2205 MeV are also included. The results show a smooth, gradual rise in $\langle A_{oon}(70°)\rangle$ and $\langle A_{oon}(80°)\rangle$ with increasing energy, with perhaps a decrease near 2800 MeV. The slope at 90° c.m. also appears to fall smoothly and slowly. Hence, no rapid energy dependence is observed over the angular and energy range of this experiment. It should be noted that much more rapid changes are seen in the spin observables $A_{oonn}=C_{NN}$ [14,24,25] and $A_{ookk}=C_{LL}$ [26–29] at 90° c.m. in this energy range. Furthermore, at 90° c.m., $A_N d\sigma/d\Omega$ contains contributions from spin-triplet partial waves only, whereas $A_{oonn}d\sigma/d\Omega$ and $A_{ookk}d\sigma/d\Omega$ have both spin-singlet and -triplet waves.

Recently, the Saclay-Geneva group performed a direct reconstruction of the pp elastic scattering amplitudes and a phase shift analysis (Ref. [21]) at four energies where many previous spin observables had been measured. The predictions for A_{oon} are shown at 2395 and 2645 MeV in Figs. 5 and 7. Also, the Arndt *et al.* PSA was recently extended from 1.6 to 2.5 GeV [30]. Their predictions at selected energies are given in Figs. 3–6, and the energy dependence of $A_{oon}(70°)$, $A_{oon}(80°)$, and $dA_{oon}/d\theta(90°)$ are shown in Figs. 9 and 10. The PSA predictions reproduce the data reasonably well and agree closely at 2395 MeV. The two solutions of the Saclay-Geneva PSA at 2645 MeV are not distinguishable for A_{oon} in the angular range measured. Note that the data from Ref. [1] and this paper are included in the data bases of Arndt *et al.* and the Saclay-Geneva group, and thus the good agreement is not surprising.

The data from run periods III and IV, shown in Figs. 3–8, will make a major contribution to the pp elastic-scattering data base. A total of 20 data sets, at 19 beam kinetic energies, and 477 different points, are included. A careful search for systematic errors, particularly from efficiency changes in the apparatus, was performed. There is good agreement with data in Ref. [1] when energies were repeated, and with other previous measurements. Many of the data sets are at energies and angles where no previous A_{oon} results exist, especially at the higher energies.

ACKNOWLEDGMENTS

We wish to express our thanks to all the operations staff of the Saturne II accelerator for excellent performance of the beams. We are indebted to C. Lechanoine-LeLuc and J. Comfort for their encouraging suggestions. This work was supported in part by the U.S. Department of Energy, Division of Nuclear Physics, Contract No. W-31-109-ENG-38, by the Swiss National Science Foundation, and by the Russian Foundation for Fundamental Physics Program 122.03.

[1] C. E. Allgower, J. Ball, L. S. Barabash, P.-Y. Beauvais, M. E. Beddo, Y. Bedfer, N. Borisov, A. Boutefnouchet, J. Bystricky, P. A. Chamouard, M. Combet, Ph. Demierre, J.-M. Fontaine, V. Ghazikhanian, D. P. Grosnick, R. Hess, Z. Janout, Z. F. Janout, V. A. Kalinnikov, T. E. Kasprzyk, Yu. M. Kazarinov, B. A. Khachaturov, R. Kunne, J. M. Lagniel, F. Lehar, J. L. Lemaire, A. de Lesquen, D. Lopiano, M. de Mali, V. N. Matafonov, G. Milleret, I. L. Pisarev, A. A. Popov, A. N. Prokofiev, D. Rapin, J. L. Sans, H. M. Spinka, Yu. A. Usov, V. V. Vikhrov, B. Vuaridel, C. A. Whitten, and A. A. Zhdanov, Phys. Rev. C **60**, 054001 (1999), preceding paper.

[2] C. E. Allgower, J. Ball, M. Beddo, Y. Bedfer, A. Boutefnouchet, J. Bystricky, P.-A. Chamouard, Ph. Demierre, J.-M. Fontaine, V. Ghazikhanian, D. Grosnick, R. Hess, Z. Janout, Z. F. Janout, V. A. Kalinnikov, T. E. Kasprzyk, B. A. Khachaturov, R. Kunne, F. Lehar, A. de Lesquen, D. Lopiano, V. N. Matafonov, I. L. Pisarev, A. A. Popov, A. N. Prokofiev, D. Rapin, J.-L. Sans, H. M. Spinka, A. Teglia, Yu. A. Usov, V. V. Vikhrov, B. Vuaridel, C. A. Whitten, and A. A. Zhdanov, Nucl. Phys. **A637**, 231 (1998).

[3] C. E. Allgower, J. Ball, L. S. Barabash, M. Beddo, Y. Bedfer, A. Boutefnouchet, J. Bystricky, P.-A. Chamouard, Ph. Demierre, J.-M. Fontaine, V. Ghazikhanian, D. Grosnick, R. Hess, Z. Janout, Z. F. Janout, V. A. Kalinnikov, T. E. Kasprzyk, Yu. M. Kazarinov, B. A. Khachaturov, R. Kunne, C. Lechanoine-LeLuc, F. Lehar, A. de Lesquen, D. Lopiano, M. de Mali, V. N. Matafonov, I. L. Pisarev, A. A. Popov, A. N. Prokofiev, D. Rapin, J.-L. Sans, H. M. Spinka, Yu. A. Usov, V. V. Vikhrov, B. Vuaridel, C. A. Whitten, and A. A. Zhdanov, Eur. Phys. J. C **5**, 453 (1998).

[4] C. E. Allgower, Ph.D. thesis, Arizona State University and Argonne National Laboratory report ANL-HEP-TR-97-71, 1997.

[5] J. Bystricky, J. Derégel, F. Lehar, A. de Lesquen, L. van Rossum, J. M. Fontaine, F. Perrot, C. A. Whitten, T. Hasegawa, C. R. Newsom, W. R. Leo, Y. Onel, S. Dalla Torre-Colautti, A. Penzo, H. Azaiez, and A. Michalowicz, Nucl. Instrum. Methods Phys. Res. A **239**, 131 (1985).

[6] R. Bernard, P. Chaumette, P. Chesny, J. Derégel, R. Duthil, J. Fabre, C. Lesmond, G. Seité, J. Ball, T. O. Niinikoski, and M. Rieubland, Nucl. Instrum. Methods Phys. Res. A **249**, 176 (1986).

[7] J. Ball, M. Combet, J.-L. Sans, B. Benda, P. Chaumette, J. Derégel, G. Durand, A. P. Dzyubak, C. Gaudron, F. Lehar, A. de Lesquen, T. E. Kasprzyk, Z. Janout, B. A. Khachaturov, V. N. Matafonov, and Yu. A. Usov, Nucl. Instrum. Methods Phys. Res. A **381**, 4 (1996).

[8] M. Arignon, J. Bystricky, J. Derégel, F. Lehar, A. de Lesquen, F. Petit, L. van Rossum, J. M. Fontaine, F. Perrot, J. Ball, and C. D. Lac, Nucl. Instrum. Methods Phys. Res. A **262**, 207 (1987).

[9] J. Ball, Ph. Chesny, M. Combet, J. M. Fontaine, R. Kunne, J. L. Sans, J. Bystricky, C. D. Lac, D. Legrand, F. Lehar, A. de Lesquen, M. de Mali, F. Perrot-Kunne, L. van Rossum, P. Bach, Ph. Demierre, G. Gaillard, R. Hess, Z. F. Janout, D. Rapin, Ph. Sormani, B. Vuaridel, J. P. Goudour, R. Binz, A. Klett, E. Rössle, H. Schmitt, L. S. Barabash, Z. Janout, V. A. Kalinnikov, Yu. M. Kazarinov, B. A. Khachaturov, V. N. Matafonov, I. L. Pisarev, A. A. Popov, Yu. A. Usov, M. Beddo, D. Grosnick, T. Kasprzyk, D. Lopiano, and H. Spinka, Nucl. Instrum. Methods Phys. Res. A **327**, 308 (1993).

[10] C. E. Allgower, J. Arvieux, P. Ausset, J. Ball, P.-Y. Beauvais, Y. Bedfer, J. Bystricky, P.-A. Chamouard, P. Demierre, J.-M. Fontaine, Z. Janout, V. A. Kalinnikov, T. E. Kasprzyk, B. A. Khachaturov, R. Kunne, J.-M. Lagniel, F. Lehar, A. de Lesquen, A. A. Popov, A. N. Prokofiev, D. Rapin, J.-L. Sans, H. M. Spinka, A. Teglia, V. V. Vikhrov, B. Vuaridel, and A. A. Zhdanov, Nucl. Instrum. Methods Phys. Res. A **399**, 171 (1997).

[11] A. Ahmidouch, P. Bach, R. Hess, R. A. Kunne, C. Lechanoine-Leluc, C. Mascarini, D. Rapin, J. Arvieux, R. Bertini, H. Catz, J. C. Faivre, F. Perrot-Kunne, F. Bradamante, and A. Martin, Nucl. Instrum. Methods Phys. Res. A **326**, 538 (1993).

[12] J. Bystricky, F. Lehar, and P. Winternitz, J. Phys. (Paris) **39**, 1 (1978).

[13] J. H. Parry, N. E. Booth, G. Conforto, R. J. Esterling, J. Scheid, D. J. Sherden, and A. Yokosawa, Phys. Rev. D **8**, 45 (1973).

[14] D. Miller, C. Wilson, R. Giese, D. Hill, K. Nield, P. Rynes, B. Sandler, and A. Yokosawa, Phys. Rev. D **16**, 2016 (1977).

[15] H. A. Neal and M. J. Longo, Phys. Rev. **161**, 1374 (1967).

[16] F. Perrot, J. M. Fontaine, F. Lehar, A. de Lesquen, J. P. Meyer, L. van Rossum, P. Chaumette, J. Derégel, J. Fabre, J. Ball, C. D. Lac, A. Michalowicz, Y. Onel, B. Aas, D. Adams, J. Bystricky, V. Ghazikhanian, G. Igo, F. Sperisen, C. A. Whitten, and A. Penzo, Nucl. Phys. **B294**, 1001 (1987).

[17] R. Diebold, D. S. Ayres, S. L. Kramer, A. J. Pawlicki, and A. B. Wicklund, Phys. Rev. Lett. **35**, 632 (1975).

[18] Y. Makdisi, M. L. Marshak, B. Mossberg, E. A. Peterson, K. Ruddick, J. B. Roberts, and R. D. Klem, Phys. Rev. Lett. **45**, 1529 (1980).

[19] H. Spinka, E. Colton, W. R. Ditzler, H. Halpern, K. Imai, R. Stanek, N. Tamura, G. Theodosiou, K. Toshioka, D. Underwood, R. Wagner, Y. Watanabe, A. Yokosawa, G. R. Burleson, W. B. Cottingame, S. J. Greene, S. Stuart, and J. J. Jarmer, Nucl. Instrum. Methods Phys. Res. **211**, 239 (1983).

[20] P. R. Bevington, M. W. McNaughton, H. B. Willard, H. W. Baer, E. Winkelmann, F. Cverna, E. P. Chamberlin, N. S. P.

King, R. R. Stevens, H. Wilmes, and M. A. Schardt, Phys. Rev. Lett. **41**, 384 (1978).

[21] J. Bystrický, C. Lechanoine-LeLuc, and F. Lehar, Eur. Phys. J. C **4**, 607 (1998).

[22] M. G. Albrow, S. Andersson/Almehed, B. Bošnjaković, C. Daum, F. C. Erné, J. P. Lagnaux, J. C. Sens, and F. Udo, Nucl. Phys. **B23**, 445 (1970).

[23] A. de Lesquen, F. Lehar, L. van Rossum, P. Chaumette, J. Derégel, J. Fabre, J. M. Fontaine, F. Perrot, P. Bach, R. Hess, Ph. Sormani, J. Ball, C. D. Lac, D. Adams, J. Bystricky, V. Ghazikhanian, and C. A. Whitten, Nucl. Phys. **B304**, 673 (1988).

[24] A. Lin, J. R. O'Fallon, L. G. Ratner, P. F. Schultz, K. Abe, D. G. Crabb, R. C. Fernow, A. D. Krisch, A. J. Salthouse, B. Sandler, and K. M. Terwilliger, Phys. Lett. **74B**, 273 (1978).

[25] F. Lehar, A. de Lesquen, J. P. Meyer, L. van Rossum, P. Chaumette, J. Derégel, J. Fabre, J.-M. Fontaine, F. Perrot, J. Ball, C. D. Lac, A. Michalowicz, Y. Onel, D. Adams, J. Bystricky, V. Ghazikhanian, C. A. Whitten, and A. Penzo, Nucl. Phys. **B294**, 1013 (1987).

[26] I. P. Auer, A. Beretvas, E. Colton, H. Halpern, D. Hill, K. Nield, B. Sandler, H. Spinka, G. Theodosiou, D. Underwood, Y. Watanabe, and A. Yokosawa, Phys. Rev. Lett. **41**, 1436 (1978).

[27] I. P. Auer, C. Chang-Fang, E. Colton, H. Halpern, D. Hill, H. Kanada, H. Spinka, N. Tamura, G. Theodosiou, K. Toshioka, D. Underwood, R. Wagner, and A. Yokosawa, Phys. Rev. Lett. **48**, 1150 (1982).

[28] F. Lehar, A. de Lesquen, L. van Rossum, J. M. Fontaine, F. Perrot, P. Chaumette, J. Derégel, J. Fabre, J. Ball, C. D. Lac, Y. Onel, A. Michalowicz, J. Bystricky, and V. Ghazikhanian, Nucl. Phys. **B296**, 535 (1988).

[29] J. M. Fontaine, F. Perrot, J. Bystricky, J. Derégel, F. Lehar, A. de Lesquen, L. van Rossum, J. Ball, and C. D. Lac, Nucl. Phys. **B321**, 299 (1989).

[30] R. A. Arndt, C. H. Oh, I. I. Strakovsky, R. L. Workman, and F. Dohrmann, Phys. Rev. C **56**, 3005 (1997), and SAID solution SP99.